Lasers in Manufacturing Conference 2023

Influence of capillary shape on spatter formation during welding with ring-core fiber systems

Felix Zaiß[a,*], Michael Haas[a,e], Jonas Wagner[a], Christian Diegel[b], Klaus Schricker[b], Jean Pierre Bergmann[b], Marc Hummel[c], Alexander Olowinski[c], Felix Beckmann[d], Julian Moosmann[d], Christian Hagenlocher[a], Thomas Graf[a]

[a]*Institut für Strahlwerkzeuge (IFSW), University of Stuttgart, Pfaffenwaldring 43, 70569 Stuttgart, Germany* [b]*Technische Universität Ilmenau, Production Technology Group, Gustav-Kirchhoff-Platz 2, 98693 Ilmenau, Germany*
[c]*RWTH Aachen University, Chair for Laser Technology LLT, Steinbachstr. 15, 52074 Aachen, Germany*
[d]*Institute of Materials Physics, Helmholtz-Zentrum Hereon, Max-Planck-Str. 1, 21502 Geesthacht, Germany*
[e]*Graduate School of Excellence advanced Manufacturing Engineering, University of Stuttgart, Nobelstr. 12, 70569 Stuttgart, Germany*

Abstract

During laser welding, the formation of spatter results from instabilities of the capillary, which are associated with adverse conditions in the melt flow surrounding the capillary and in the vapor flow at the capillary opening.
A change of the characteristics of these flows in the melt pool and in the capillary requires a change of the shape of the capillary and/or the surrounding melt pool. In order to influence the stabilize the capillary the intensity distribution was varied by means of a ring-core fiber system. Analysis of the resulting welds shows a significant effect of the intensity distribution on the stability of the capillary shape and considerable changes in the melt flow direction and velocity. These findings identified an optimum capillary shape, which results from a specific power share in the ring-core fiber combination.

Keywords: Laser welding; spatter formation; synchrotron; x-ray imaging; beam shaping

* Corresponding author. Tel.: +49-711-685-63071; fax: +49-711-685-66842.
E-mail address: felix.zaiss@ifsw.uni-stuttgart.de.

1. Introduction

During laser welding, with sufficient intensity of the laser beam on the sample's surface, a capillary is formed by the recoil pressure of the evaporated metal. This type of welding is called deep-penetration welding, since the formation of a capillary enables deep and narrow welds. During deep penetration welding metal droplets (spatter) may be ejected out of the capillary or the melt pool and can land on the component itself or the clamping device and cause damage to the product. The detachment of spatters from the melt requires a sufficient force. In literature one can find three major mechanisms associated to the formation of spatter.

One, the formation of spatter is attributed to fluctuations and collapses of the capillary as described by Volpp, 2017. The avoidance of such spatter requires a stable capillary shape, which is addressed by beam shaping strategies in M. Jarwitz et al., 2019 or by highspeed welding in Fetzer et al., 2018.

Two, the formation of spatter is attributed to the friction between the outflowing metal vapor and the liquid surface of the inner wall of the capillary as described by Kaplan and Powell, 2011. The higher the outflowing metal vapor velocity the more friction is present to detach molten particles from the melt pool as described by Weberpals and Dausinger, 2008. One way to decrease the vapor velocity is to widen the diameter of the capillary opening. A volumetric flow $\dot{V}$ of the metal vapor, as described by Bernoulli shown in Decher, 2022 can be described as a flow cross-section *A* passing a distance *d* over time *t*.

$$\dot{V} = \frac{d \cdot A}{t} = u_{vap} \cdot A \qquad (1)$$

Assuming a constant volumetric flow, the flow velocity u_{vap} decreases when the flow cross-section A of the capillary opening increases. A reduced vapor velocity v_{vap} results in less friction between the metal vapor and the inner wall of the capillary.

Third, the formation of spatter is connected with the melt flow velocity around the capillary as described by Eriksson et al., 2011. During deep penetration welding, the liquid in front of the capillary flows towards the back of the melt pool and passes the capillary through the channel between the side wall of the capillary and the side of the weld pool, as stated by Beck, 1996. According to Beck, 1996 the melt flow velocities are at maximum in this channel and the maximum melt flow velocity

$$u_{melt,max} = u_{weld}\left(2 \cdot \frac{B_K}{B_K - r_{kap}} - 1\right) \qquad (2)$$

depends on the width of the melt pool B_K at the laser position, the radius of the capillary r_{kap} and the welding velocity u_{weld}.Furthermore the melt flow velocities around the capillary increase with the welding speed as shown by equation (2) and by Berger and Hügel, 2013.

Assuming a constant or increasing volumetric melt flow in the case of increasing the welding velocity, as described by equation (2) a reduction of the channel's cross section significantly increases the melt flow velocity. In order to decrease these high melt flow velocities, the channel's cross section between the side of the capillary and the side of the weld pool has to be extended. This can be addressed by heating the sample at the surface surrounding of the capillary, as presented by Nagel et al., 2018.

From the present literature one can conclude that the reduction of spatter formation requires an optimization of the capillary shape to and reduce fluctuations and collapses of the capillary, as well as influence

of the vapor and the melt flow mechanisms. These topics can be addressed by shaping the intensity distribution with a core-ring-fiber-system.

The aim of this work is reducing spatter formation by influencing the major mechanisms, which effect capillary shape and melt pool flow characteristics, by means of ring-core intensity distributions. In order to analyze the effects of the intensity distribution changes, synchrotron X-ray imaging was used to determine the shape of the capillary and highspeed cameras to analyze the generation of spatter. To investigate changes in the melt bead formation and therefore the melt flow mechanisms, metallographic cross sections of the welded samples were made.

2. Setup

The generation of spatter and the shape of the capillary during deep penetration welding of stainless steel 1.4301 was investigated using a “HighLight FL-ARM” laser from Coherent, which generates a beam with a wavelength of 1.070 µm. The laser beam is delivered to the processing optics by a multi-core fiber with a core fiber with a diameter of 25 µm in the core and a surrounding ring fiber with a diameter of 125 µm. This allows for a range of ring-core intensity distributions on the surface of sample as described in detail in Hollatz et al., 2023 - 2023. The power can be modulated independently up to maximum laser power of 1500 W in the core fiber and 2400 W in the ring fiber. Using processing optics with an aspect ratio of 2.7, the beam of the core fiber was focused on the sample`s surface to a spot diameter of 67.5 µm and the beam of the ring fiber was focused to an outer diameter of 450 µm. The relative movement between sample and laser beam was achieved by moving the sample with a feed rate of 12 m/min. The intensity distribution was controlled by varying the power which transmitted in the core fiber and ring fiber, as listed in Table 1. The relation between the power in the core fiber and the power in the ring fiber is given by the ring-core power ratios, listed in the first column of Table 1. The aim of the experiment was to observe welding characteristics at ring-core power ratios of 1:0, 0.5:0.5.

The Setup of the X-ray imaging system at Deutsches Elektronen-Synchrotron (DESY) is presented in detail in Kaufmann et al., 2023. To get high framerates with high contrast the samples had a thickness of 2 mm and the frame rate of the camera (i-SPEED 727, iX Cameras) was set to 10 kHz, with a spatial resolution of 390 pixels/mm. To convert the X-ray radiation into visible light a GaGG scintillator crystal was used with a thickness of 1.6 µm.

The X-ray recordings were post-processed with a flat-field correction, to increase contrast, as described in Wagner et al., 2021.

The high-speed camera (OS8, IDT Vision) to record the spatter was equipped with a Navitar zoom lens and was arranged perpendicular to the welding direction with and an angle of 9 ° from the sample surface. To be able to track fast and small spatters, the frame rate was set to 8 kHz with a spatial resolution of 800 pixels/mm.

In order to investigate the influence of the shape of the capillary and especially the capillary opening on the formation of spatters, the penetration depth of the capillary was kept constant at about 900 µm.

Table 1 lists the relevant laser powers of core and ring fiber at a welding velocity of 12 m/min and at different intensity distributions.

Table 1. Investigated laser power distributions

Laser power configurations in core and ring fiber	Laser power core fiber [W]	Laser power ring fiber [W]
100 % core – 0 % ring	400	0
50 % core – 50 % ring	390	390

3. Results

The image sequences of the X-ray and high-speed videos were evaluated to determine the influence of the intensity distributions on the shape of the capillary and the melt, and the ejection of spatter.

To quantify the spatter formation with regard of the number and preferred direction of the spatter the maximum gray scale values of each frame in a video sequence were analyzed after the process achieved steady state conditions.

Fig. 1 represents the formation of spatter by the local grey scale maxima of a high speed video during deep penetration welding. The welding direction is towards the right, with a welding velocity of 12 m/min and a laser power of 400 W in the core fiber. The ring fiber was turned off in this experiment. Fig. 1a shows the generated spatter as an overlay of the maximum gray scale value of 100 images, which corresponds to a welding distance of 10 mm. The white spots represent spatter, which can be detected by the high speed camera due to the thermal emissions of the hot droplets. The trajectory of a spatter can be determined by following the in-line spots in the image. The red line represents the laser beam hitting the surface of the sample with an angle of 7 degree.

Fig 1b shows describes a similar image but at a different welding configuration, in this case with the ring fiber turned on. The laser power parameters were 390 W in the core fiber and 390 W in the ring fiber.

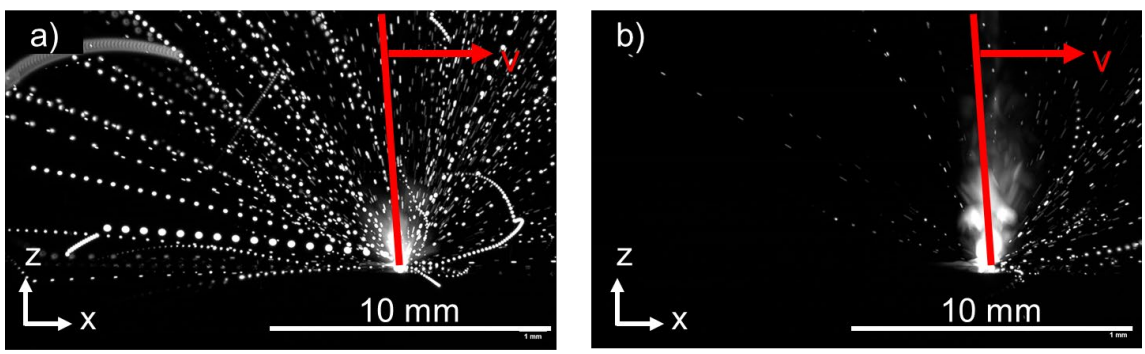

Fig. 1. The formation of spatter during a welding distance of 10 mm as a stacked image of the maximum grey scale values of the recordings. In (a), maximum stack image of the laser configuration with 400 W in the core fiber is shown. In (b), the laser configuration with 390 W in the ring fiber and 390 W in the core fiber is shown.

In case of combining ring and core fiber as listed in the second row of Table 1, the direction and volume of the ejected spatter was significantly reduced.

As a next step, the capillary shape from the X-ray recordings was investigated. Fig. 2 shows the X-ray recordings of the capillary shape at time interval of 15 ms during the weld. The welding direction is towards the right, with a welding speed of 12 m/min and a laser power of 400 W in the core fiber. The ring fiber was turned off in this experiment. In Fig. 2a an elongated structure in a lighter grey is visible, representing the capillary. The shape of the capillary is long and narrow. b shows the capillary shape after 7.5 ms and the depth decreases by about the half. C show the capillary 7.5 ms after b) and capillary depth increased again like can be seen in a). Each frame of the recording was post-processed using the Flat-Field corrections method described in Wagner et al., 2021.

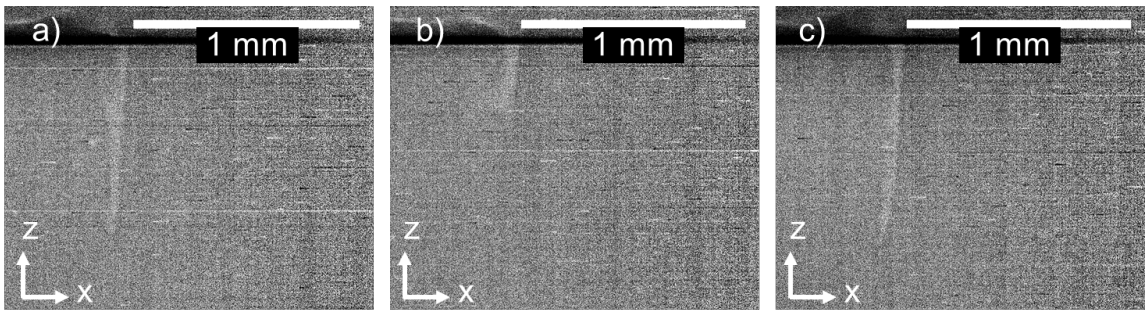

Fig. 2. X-ray recordings of the capillary shape in a time interval of 15 ms. (a) shows a narrow and deep capillary. (b) shows a decrease of the capillary depth at 7.5 ms after (a). (c) shows an increase of the capillary depth and a similar shape as seen in (a).

The frame sequence shows a collapse of the capillary during the laser beam welding process. During a short period of time, the depth of the capillary decreased by half. These collapses cause turbulence and disturbances in the melt pool, contributing to the formation of spatters, as presented in Fig. 1a.

Figure 3 shows the same setup with the same post-processing methods as Fig. 2, but this time the ring fiber had a power of 390 W, with a spot diameter of 450 µm on the sample's surface, as listed in the second row of Table 1. Once again, the images show the capillary shape in a sequence with a separation of 7.5 ms. The depth of the capillary in a, b and c is almost identical.

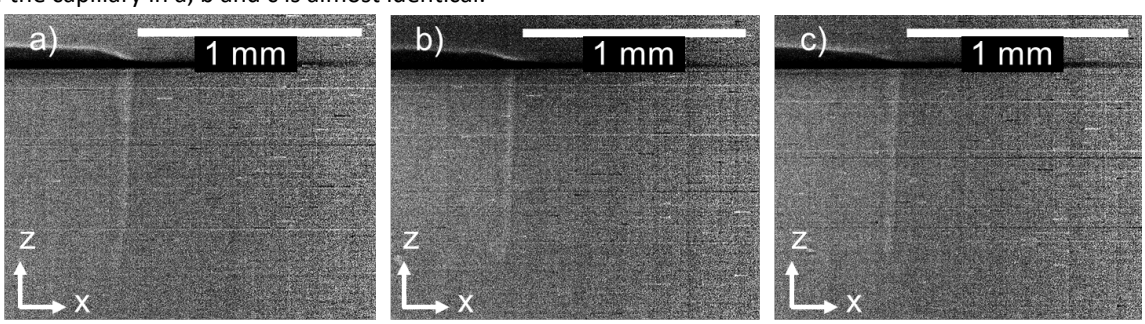

Fig. 3. X-ray recordings of the capillary shape in a time interval of 15 ms. All capillary shapes look similar during the welding process.

With the ring fiber turned on the stability of the capillary was improved. Otherwise, the capillary shapes from Fig. 2c and Fig. 3b look very similar, which supports the assumption that the only difference in the welds regarding the capillary is the stability.

To investigate the influence of the different intensity distributions on the melt pool, metallographic cross sections were made. Fig. 4 shows the cross sections for the investigated intensity distributions of Table 1. The cuts were made after the half weld length welding process. After cutting the sample, the surface was mechanically polished and etched for the sake of visibility. The image of the cross section was captured by an optical microscope and the outer contour of the melt pool was outlined for better visibility. Fig. 4a shows the cross section of the weld with only the core fiber turned on. The melt pool is narrow and deep as seen in Fig. 2a. Following the outline of the melt pool from downwards, one can see that it has a meandering shape, indicative of instability. The penetration depth is 850 µm and the width of the melt pool at the sample's surface is 276 µm. Fig. 4b shows the cross section of the weld with an optimized intensity distribution, which results from the conditions presented in the second row of Table1. The width of the melt pool in the upper region is clearly increased. The widened melt pool narrows with increasing depth until a narrow capillary shape as seen

in Fig 4a remains. The penetration depth is 930 µm and the width of the melt pool at the sample's surface is 447 µm.

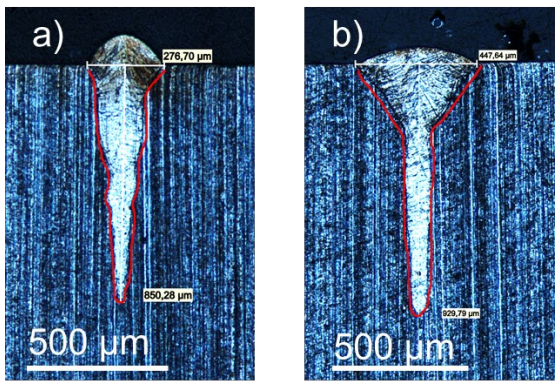

Fig. 4. Metallographically cross sections of the welded sample. The influence of different ring-core configurations on the melt pool is clearly visible. (a) shows a narrow melt pool. (b) shows a widened melt pool at the sample's surface narrowing width increasing weld depth.

The influence of the ring fiber is clearly visible. The profile is stable and the widening of the melt pool at the top indicates a change of the melt flow characteristics in this area. With reference to equation (2) the increase of the melt pool by the factor of 1.62, as seen in Fig. 4, and the same capillary shape, as seen in Fig. 3 and Fig. 2, should reduce the maximum flow velocity by 27 %. This reduction of melt flow velocity, in combination with the increased stability of the capillary contributes to a reduced formation of spatter as seen in Fig. 1b.

4. Summary

Deep penetration welds in steel at 12 m/min with different intensity distributions were conducted. The influence on the stability of the capillary shape and the melt and vapor flow was investigated, in order to reduce the formation of spatter. To record the fluctuations of the capillary and during the welding process an X-ray imaging system was used and recorded using Highspeed Cameras. The formation of spatter was recorded with a high speed camera orientated perpendicular to the welding direction. Metallographic cross sections were used to investigate the influence of the intensity distribution on the weld.

The X-ray recordings show that when welding with power in the core fiber the capillary is narrow,unstable and collapses frequently. When the ring fiber was turned on, the capillary shape looked the same but the collapses could be reduced. The spatter recordings show a significant reduction of spatter in case of optimizing the instensity distribution with the ring fiber. Additionally, the cross sections show a widening of the melt pool at the sample's surface in case of an enhanced intensity distribution.

Further investigation will focus on the optimization of the ring/core power ratio and quantify the formation of spatter by angle and direction of the spatter. In Addition, the X-ray recording can be used to investigate the influence of the capillary shape and the outflowing metal vapor on the formation of spatter.

Acknowledgements

The presented investigations were carried out in cooperation with DESY in Hamburg and with RWTH Aachen University within the framework of the Collaborative Research Centre SFB1120-236616214 "Bauteilpräzision durch Beherrschung von Schmelze und Erstarrung in Produktionsprozessen" and funded by the Deutsche

Forschungsgemeinschaft e.V. (DFG, German Research Foundation). We acknowledge DESY (Hamburg, Germany), a member of the Helmholtz Association HGF, for the provision of experimental facilities. Parts of this research were carried out at PETRA III and we would like to thank F. Beckmann and J. Moosmann for assistance in using P07 EH4. Beamtime was allocated for proposal I-20210713.The sponsorship and support are gratefully acknowledged.

The presented work was funded by the Deutsche Forschungsgemeinschaft (DFG, German Research Foundation) – 503306266.

References

Beck M., 1996. Modellierung des Lasertiefschweißens

Berger P., Hügel H., 2013. Fluid Dynamic Effects in Keyhole Welding – An Attempt to Characterize Different Regimes. Physics Procedia 41, pp 216–224. doi: 10.1016/j.phpro.2013.03.072

Decher (2022). The Vortex and The Jet, 1st edn. Springer Singapore

Eriksson I., Powell J., Kaplan A. F. H., 2011. Melt flow measurement inside the keyhole during laser welding. 13th NOLAMP Conference : 13th Conference on Laser Materials Proce Nordic Countries

Fetzer F., Hagenlocher C., Weber R., 2018. High Power, High Speed, High Quality. LTJ 15, pp 28–31. doi: 10.1002/latj.201800017

Hollatz S., Hummel M., Lach M.-C., Olowinsky A., Gillner A., Häfner C., Beckmann F., Moosmann J., 2023 - 2023. Influence of ring-shaped laser beam during welding of AW-5083 and AW-6082. In: Kleine KR, Kaierle S (eds) High-Power Laser Materials Processing: Applications, Diagnostics, and Systems XII. SPIE, p 24

Kaplan A. F. H., Powell J., 2011. Spatter in laser welding. Journal of Laser Applications 23, p 32005. doi: 10.2351/1.3597830

Kaufmann F., Forster C., Hummel M., Olowinsky A., Beckmann F., Moosmann J., Roth S., Schmidt M., 2023. Characterization of Vapor Capillary Geometry in Laser Beam Welding of Copper with 515 nm and 1030 nm Laser Beam Sources by Means of In Situ Synchrotron X-ray Imaging. Metals 13, p 135. doi: 10.3390/met13010135

M. Jarwitz, J. Lind, R. Weber, T. Graf, 2019. Influence of superimposed intensity distributions on the welding process and the spatter behavior during laser welding of steel

Nagel F., Brömme L., Bergmann J. P., 2018. Description of the influence of two laser intensities on the spatter formation on laser welding of steel. Procedia CIRP 74, pp 475–480. doi: 10.1016/j.procir.2018.08.147

Volpp J., 2017. Keyhole stability during laser welding—Part II: process pores and spatters. Prod. Eng. Res. Devel. 11, pp 9–18. doi: 10.1007/s11740-016-0705-4

Wagner J., Hagenlocher C., Hummel M., Olowinsky A., Weber R., Graf T., 2021. Synchrotron X-ray Analysis of the Influence of the Magnesium Content on the Absorptance during Full-Penetration Laser Welding of Aluminum. Metals 11, p 797. doi: 10.3390/met11050797

Weberpals J., Dausinger F., 2008. Fundamental understanding of spatter behavior at laser welding of steel. In: International Congress on Applications of Lasers & Electro-Optics. Laser Institute of America, p 704